

---

This is an electronic reprint of the original article.  
This reprint may differ from the original in pagination and typographic detail.

Soldano, Caterina; Laouadi, Ornella; Kornienko, Vladimir; Gallegos-Rosas, Katherine; Azari, Amirhossein

## Electroplex Emission in TADF-Based Organic Light-Emitting Transistors

*Published in:*  
ACS Photonics

*DOI:*  
[10.1021/acsp Photonics.5c01335](https://doi.org/10.1021/acsp Photonics.5c01335)

Published: 19/11/2025

*Document Version*  
Publisher's PDF, also known as Version of record

*Published under the following license:*  
CC BY

*Please cite the original version:*  
Soldano, C., Laouadi, O., Kornienko, V., Gallegos-Rosas, K., & Azari, A. (2025). Electroplex Emission in TADF-Based Organic Light-Emitting Transistors. *ACS Photonics*, 12(11), 5958–5969.  
<https://doi.org/10.1021/acsp Photonics.5c01335>

---

This material is protected by copyright and other intellectual property rights, and duplication or sale of all or part of any of the repository collections is not permitted, except that material may be duplicated by you for your research use or educational purposes in electronic or print form. You must obtain permission for any other use. Electronic or print copies may not be offered, whether for sale or otherwise to anyone who is not an authorised user.

# Electroplex Emission in TADF-Based Organic Light-Emitting Transistors

Caterina Soldano,\* Ornella Laouadi, Vladimir Kornienko, Katherine Gallegos-Rosas, and Amirhossein Azari



Cite This: *ACS Photonics* 2025, 12, 5958–5969



Read Online

ACCESS |



Metrics & More



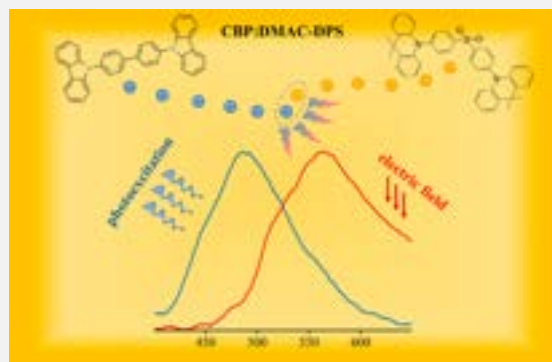
Article Recommendations



Supporting Information

**ABSTRACT:** Thermally activated delayed fluorescence (TADF) offers promising routes to enhance the efficiency of organic light-emitting devices by enabling utilization of both triplet and singlet excitons. In this study, we investigate the performance of multilayer organic heterostructures incorporating the TADF emitter DMAC-DPS blended with CBP, under field-effect charge transport conditions in transistor-based devices. We systematically studied the optical and electronic properties of emissive blends within the device architecture. Two key findings emerge from this study: (a) a DMAC-DPS concentration of 15% yields the highest electroluminescence efficiency, which we attribute to balanced charge transport within the emissive layer, and (b) electrical excitation induces a pronounced red shift in the emission spectrum, suggesting electroplex formation at the interface between the emissive blend and the *n*-type semiconductor. These results highlight the critical role of balanced charge transport and interfacial interactions for the understanding of light generation mechanisms and overall improvement of the device performances while offering new insights into the design of TADF-based light-emitting transistors.

**KEYWORDS:** Organic light-emitting transistor (OLET), field-effect devices, emissive layer, Thermally-Activated Delayed Fluorescence (TADF) molecules, DMAC-DPS, light emission



## INTRODUCTION

Organic materials and devices have continuously attracted significant attention as potential low-cost, lightweight, semi-transparent, and customizable solutions for a wide variety of applications in fields such as wearable and flexible electronics. In these fields, conventional inorganic and complementary metal-oxide semiconductor (CMOS)-based technologies are currently facing major bottlenecks due to the shortage and brittleness of materials. Organic materials can be engineered through synthesis to achieve a broad range of optical and electronic properties to address specific functionalities and they are generally inexpensive, biocompatible, easier to be integrated in low-cost manufacturing processes and environmentally friendly, when coming to their *end-of-life* disposal.<sup>1–3</sup>

For example, organic light-emitting devices have been exploited for applications such as solid-state lighting and displays due to their high electroluminescence efficiency and brightness and the ability to be manufactured on various substrates. In fluorescent emitters, light is emitted from singlet excited states, with the internal quantum efficiency (IQE) limited to 25%, determined by the 1:3 singlet-to-triplet ratio resulting from the charge recombination (holes and electrons). At room temperature, the remaining 75% of charge recombination events due to triplets is typically not emissive,

thus leading to major losses in the devices. Heavy-metal-containing phosphorescent emitting materials have been proposed as exciton harvesters, with the emission occurring from both the singlet and triplet excited states arising from enhanced spin–orbit coupling (SOC) *via* enhanced inter-system crossing (ISC).<sup>4</sup> However, during device operation, these materials also exhibit some drawbacks, including color instability (especially for emission in the blue region of the spectrum)<sup>5</sup> and cost (related to synthesis/fabrication). Therefore, they are not the optimal candidates when high-production output is required, such as in lighting and display industries, also giving potential future scarcity of the global supplies of rare-earth elements.<sup>6</sup>

Several mechanisms have been suggested to harvest triplets in organic luminescent materials such as hot exciton<sup>7</sup> and thermally activated delayed fluorescence (TADF) materials.<sup>8,9</sup> In the latter one, as it occurs in fluorescent emitters, the light

Received: June 10, 2025

Revised: September 27, 2025

Accepted: October 1, 2025

Published: October 18, 2025



emission arises from the singlet excited state; if the singlet–triplet energy gap  $\Delta E_{ST}$  is small enough, this allows for efficient upconversion of triplet excitons into singlet excitons through reverse intersystem crossing (rISC) by means of thermal activation.<sup>10</sup> This can then lead to an IQE of nearly 100% compared to the 25% in conventional singlet fluorescent emitters.

Over the past decade, the TADF mechanism has led to significant improvements in the efficiency of light-emitting devices (mainly OLEDs) with high brightness and *state-of-the-art* color coordinates.<sup>11–13</sup> TADF molecules with a small singlet–triplet energy splitting can be designed and synthesized using covalently linked electron donor and acceptor units, creating a strong charge transfer (CT) character and minimal overlap between the highest occupied molecular orbital (HOMO) and lowest unoccupied molecular orbital (LUMO), reducing the energy gap between the singlet and triplet states. Since the first report on thermally activated delayed fluorescence by Adachi et al. in 2012,<sup>14</sup> TADF molecules have been successfully exploited in emissive layers (EMLs) in organic light-emitting diodes (OLEDs), from either vacuum thermal evaporation or solution-based processing.<sup>15</sup> Zhao et al. demonstrated that anchoring flexible chains terminating in bipolar 9,9'-spiro[fluorene] can promote a higher degree of molecular planarity, leading to improved horizontal dipole alignment and increased photoluminescence in neat films. As a result of this molecular design, nondoped, solution-processed OLEDs demonstrate a record-high external quantum efficiency exceeding 30%.<sup>16</sup> Host(s)–guest configurations are commonly adopted in emissive layers: these are optimized to suppress concentration quenching, resulting from long-lived triplet excitons; on the other hand, introducing host matrices complicates device fabrication and increases the overall fabrication costs.<sup>17</sup> Thermal stability of thermally activated delayed fluorescent materials is similar to that of fluorescent materials, while their internal quantum efficiency (IQE) can be comparable to that of phosphorescent ones, i.e., nearly 100% IQE (by harvesting both singlet and triplet excitons).<sup>18,19</sup> Chen et al. demonstrated a green TADF emitter with an extended linear donor–acceptor–donor structure designed to simultaneously enhance horizontal emitting dipole orientation, reverse intersystem crossing rate ( $\sim 10^6/s$ ), and photoluminescence quantum yield (PLQY;  $\sim 95\%$ ). The resulting OLED exhibited an EQE of nearly 40% without external light-extraction structure, along with a power efficiency ( $>100$  lm/W) and reduced efficiency roll-off.<sup>20</sup> Jiang et al. introduced bulky carbazolyl units to separate the planar TADF molecule core to reduce quenching of the emission, achieving an EQE of 40% with a narrow emission (fwhm = 25 nm), which is so far the highest reported for a single OLED combining high efficiency and spectral purity. Further, those devices retain an EQE above 30% even at 30 wt % doping, demonstrating excellent doping insensitivity and stability.<sup>21</sup> Recent studies also demonstrated enhanced stability in OLEDs using blue TADF when compared to blue phosphorescent; this holds great potentials for a final solution to the stability challenges in highly efficient blue OLEDs.<sup>22,23</sup> However, further studies are still needed, considering the still considerably shorter lifetime than that of green devices to date.<sup>24,25</sup>

Organic light-emitting transistors (OLETs) combine in a single device the switching capability of a *field-effect* transistor<sup>26</sup> and light-emitting (sensing) function of an

OLED; fundamentally different from OLEDs in structure and operation, charge transport occurs horizontally in OLETs compared to vertically in OLEDs.<sup>27,28</sup> Organic light-emitting field-effect devices are also capable of light spatial modulation within the device through the control of both source-drain and gate bias, leading to top-emission (as well as bottom emission if gate is optical transparent), differently from the diode counterpart.<sup>29</sup> This also supports an effective separation between the exciton population and the charge carriers within the transistor, thus limiting the quenching phenomena. The presence of the dielectric layer also renders the device less sensitive to pinholes and shorts between electrodes, as compared to that of the case for the case of OLEDs. Undoubtedly, OLETs offer for example a route to remarkably simplified display pixel circuitry, as no driving TFTs are potentially needed when OLETs are used as light source in an active-matrix display, thus representing a key advantage to less expensive large-scale production of organic active-matrix electroluminescence displays (AM-OLETs).<sup>30,31</sup> Beyond displays, OLETs are increasingly explored for applications in optical sensors, photonic circuits, and biointegrated electronics, owing to their solution processability, mechanical flexibility, and compatibility with large-area, low-cost fabrication methods.<sup>32</sup>

To achieve organic light-emitting transistors with high-performance requires both large source-drain currents at low biases and large light output; this can be addressed in several ways by optimizing various components, including high-mobility and high-performance organic semiconductors,<sup>33,34</sup> device architecture (multilayer heterostructures, nonplanar electrodes, injection layers, vertical transistor geometry),<sup>35</sup> luminescent materials, with high fluorescence and PLQY in solid state and tunable color coordinates,<sup>36</sup> dielectric layer (capacitance per unit area and favorable interface with semiconductor layer),<sup>37</sup> and control over interfacial and bulk trap states at different interfaces within heterostructured devices.<sup>38</sup>

While planar multilayer and single crystal OLETs have achieved modest efficiencies,<sup>39,40</sup> the field has advanced significantly with novel architectures such as vertical organic permeable base light-emitting transistors (OPB-LETs), introduced by Wu et al., which achieved devices operating below 5 V with exceptionally high external quantum efficiencies (24.6% for green, 19.6% for red, and 11.8% for blue emission). This performance results from the combination of a nanoporous permeable base electrode and an integrated optical microcavity that precisely balance charge injection and maximize light output.<sup>41</sup> Further, a hybrid architecture combining colloidal quantum dots and light-emitting field-effect transistor (QD-HLET) using solution-processed InScO/ZnO as transport layers delivered a peak EQE of 22.8%, high brightness ( $\sim 145,000$  cd/m<sup>2</sup>) and mobility ( $\sim 3.1$  cm<sup>2</sup>/(V s)), and an operational lifetime exceeding 150,000 h at 100 cd/m<sup>2</sup>.<sup>42</sup>

Recently, Lee et al. demonstrated through optical simulation the potential to reach an efficiency value of approximately 40% by carefully engineering the thicknesses and refractive indices of both the transporting layers and the gate dielectric material in multilayer heterostructure OLETs.<sup>43</sup>

Available studies in the literature on light-emitting field-effect transistors using TADF molecules have been very limited.<sup>10</sup> Initial reports on light-emitting transistors employed a thermally activated exciplex system based on the TCTA:B3PYMPM donor–acceptor blend rather than a

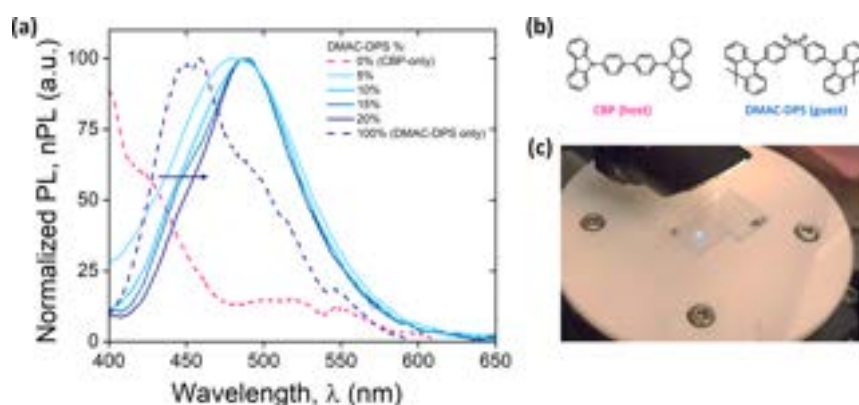


**Figure 1.** (a) Normalized photoluminescence (nPL) for CBP:DMAC-DPS emissive blends as a function of DMAC-DPS content within the blend. Photoluminescence of pure CBP and DMAC-DPS films are also reported. (b) Chemical formula of the CBP (host) and the DMAC-DPS (guest). (c) Optical image of one of our representative blend films on quartz when optically excited.

single-molecule TADF emitter. These devices achieved moderate performances, including an exciton utilization efficiency of 60.3%, a maximum EQE of 0.93% and luminance exceeding 1000  $\text{cd}/\text{m}^2$ .<sup>44</sup> The first demonstration of the use of OLETs employing intramolecular TADF material used 4CzIPN as the emissive layer. Both *p*-type and *n*-type transistor configurations were explored, yielding EQEs around 0.1% and brightness levels ranging from 100 to 1000  $\text{cd}/\text{m}^2$ , depending on the electrode polarity and configuration. The relatively low efficiency in these devices was attributed to exciton recombination occurring beneath the metallic electrode, which limits outcoupling.<sup>45</sup> Laterally integrated organic light-emitting transistors incorporating intrinsic optical microcavities have shown potential for both high color purity and efficiency. In fact, Miao et al. reported OLET devices with ultranarrow electroluminescence line widths, with fwhm values of 13 nm (blue), 14 nm (green), and 18 nm (red), achieving a high color purity and high current efficiencies of 37  $\text{cd}/\text{A}$  (green) and 26  $\text{cd}/\text{A}$  (red).<sup>46</sup> Ahmad et al. developed highly efficient light-emitting field-effect transistors by solution processes using the TADF emitter ACRXTN, with devices exhibiting external quantum efficiencies of  $\sim 1\%$ , high ON/OFF ratios ( $\sim 10^5$ ), and low bias operation ( $\sim 22$  V), with minimal EQE roll-off at brightness levels of  $\sim 1500$   $\text{cd}/\text{m}^2$ . Optical simulations suggested that the lower EQE in the case of the OLET primarily arises from reduced out-coupling efficiency ( $\sim 0.8\%$ ), when compared to OLEDs ( $\sim 24\%$ ).<sup>47</sup>

Here we report on the behavior of 10,10'-(4,4'-sulfonylbis(4,1-phenylene))bis(9,9-dimethyl-9,10-dihydroacridine) (DMAC-DPS), in combination with 4,4'-bis(N-carbazolyl)-1,1'-biphenyl 4,4'-bis(N-carbazolyl)-1,1'-biphenyl (CBP), used as a host-guest system within a multilayer heterostructure in a transistor device architecture. DMAC-DPS is one of the most used donor groups for the design of highly efficient TADF emitters, due to its planar rigid configuration and strong electron-donating capability; it shows a high PLQY (ratio of photons absorbed to photons emitted through fluorescence) of 88% in neat films and HOMO and LUMO values of  $-5.92$  and  $-2.92$  eV, respectively.<sup>48</sup> Engineering the length of the alkyl chains<sup>49</sup> or the acceptor group<sup>50</sup> has been shown to tune emission properties to realize efficient devices. In addition to delayed fluorescence, DMAC-DPS and DMAC-based compounds also exhibit further interesting emission properties, including aggregation-induced emission (AIE), mechanochromic response (ML), and room-temperature phosphorescence

(RTP).<sup>51</sup> On the other hand, CBP is also a very common host material in the solid state, given its broad energy gap (HOMO:  $-6.0$  eV, LUMO:  $-2.9$  eV), making it suitable for a very broad range of emitters within the entire visible spectrum.<sup>52</sup> While  $T_1$  energy values (with respect to the ground state) of CBP ( $-2.6$  eV) and DMAC-DPS ( $-2.91$  eV) are energetically close (0.3 eV difference), the LUMO and HOMO of DMAC-DPS can potentially form electron and hole traps for direct charge and exciton capture.<sup>53</sup>

In this work, we fabricated and compared different emissive blends (different DMAC-DPS contents) integrated in a multilayer heterostructure architecture, for which we found the most efficient light generation process for the emissive blend containing 15% DMAC-DPS and we interpreted our findings in terms of the (balanced) transport of the blend itself combined with an improved direct electron injection within the device structure. Further, we also found a red-shifted emission in the case of electrical excitation when compared to photoexcitation, which we suggest is the result of electroplex formation at the interface between the emissive layer and the electron-transporting semiconductor. Our study not only demonstrates that TADF molecules can be successfully implemented in *field-effect* devices but also provides further insights on the role played by the charge transport occurring in the emissive layer in the light generation process, thus suggesting additional potential avenues to engineer and improve the overall device efficiency.

## RESULTS AND DISCUSSION

**Photoexcitation in CBP:DMAC-DPS Blends.** Figure 1a shows the normalized photoluminescence (nPL) spectra for TADF-based blends deposited on a quartz substrate, containing CBP as a host and different concentrations of the guest DMAC-DPS (5, 10, 15 and 20%). All blends have a thickness of 60 nm; corresponding spectra for both CBP (60 nm) and DMAC-DPS (60 nm) neat films are also included as reference (dashed lines). Molecular structures of both host and guest materials are presented in Figure 1b. We refer the reader to the Supporting Information for a brief description of the TADF mechanism (Figure S1, Supporting Information). All spectra show a broad emission due to strong charge-transfer (CT) characteristics, with the main peak at around 460 nm (Figure 1c). The overall shape of the spectra is consistent with the fluorescence signal of DMAC-DPS both in solution and in the solid state (neat film and blends<sup>21</sup>) as well as the double-

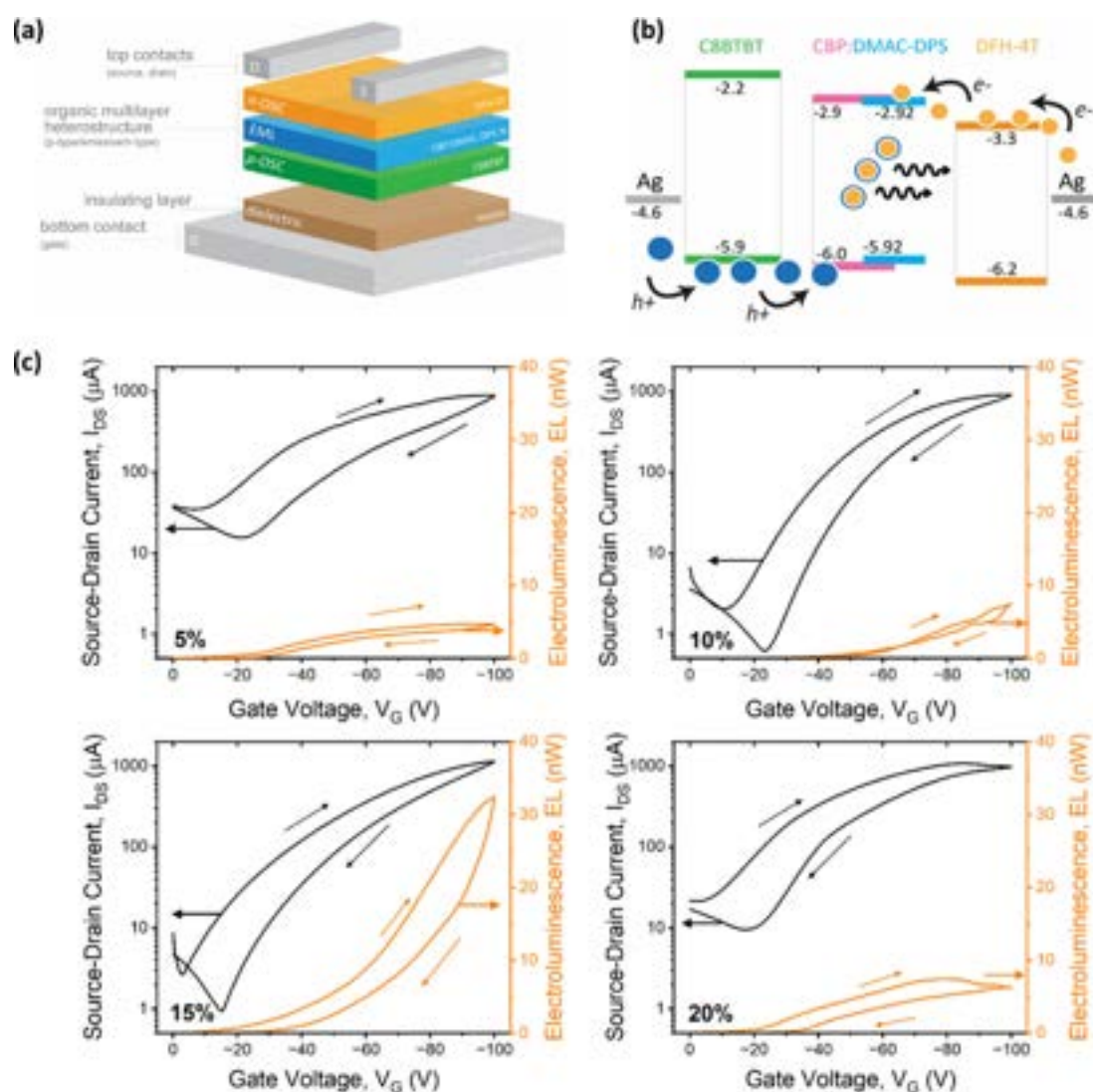


**Figure 2.** (a) Schematic of the multilayer transistor heterostructure and (b) its corresponding energy levels. (c) Saturation transfer curves ( $I_{DS}$  vs  $V_G$  @  $V_{DS} = V_{DS,max} = -100$  V) for 3L OLET with CBP:DMAC-DPS emissive layer with DMAC-DPS contents of 5, 10, 15 and 20% (as labeled). The right  $y$ -axis refers to the measured light output (bottom emission). The direction of sweeps is also indicated.

peaked structure of CBP neat film.<sup>54</sup> We observed a red-shift of the main emission peak when DMAC-DPS is within the blend as compared to neat film (DMAC-DPS only), which tends to increase with increasing guest content within the blend (Figure S2, Supporting Information); further, the contribution from CBP decreases, indicating the role of CBP in the energy transfer in the host–guest system. This suggests that the exciton density depends (increases) from the concentrations of DMAC-DPS. Except for the blend with 5% DMAC-DPS content, the variation of the main emission peak among the different DMAC-DPS concentration is within experimental error (<1–2 nm), suggesting that PL for CBP:DMAC-DPS is overall nearly concentration independent, as previously reported for DMAC-DPS in blends using for example mCP as host.<sup>55</sup> Further, we observed a small variation of the width of the main emission peak, due to the increased dispersion of the emission energies produced.<sup>56</sup> This could be related to the sterically constrained motion of the host molecules, which can lead to strong, permanent local electric fields, leading to a spectral shift of individual molecules.

**Multilayer Light-Emitting Field-Effect Transistor Using CBP:DMAC-DPS Blends as Emissive Layer.** Figure 2a shows the schematics of our bottom-gate/top-contacts (BG-TC) transistors. We used a poly(methyl-methacrylate) (PMMA) layer with a thickness of approximately 430 nm as gate dielectric; this was spin-coated and annealed on a hot plate in air on top of the transparent gate (G) electrode (indium tin oxide, ITO). PMMA was chosen as a polymer dielectric layer since it offers a suitable interface for organic materials in terms of surface roughness.<sup>57</sup> The multilayer active region consists of three stacked organic layers (from bottom to top): (a) the hole-transporting layer (2,7-dioctyl[1]-benzothieno[3,2-*b*][1]benzothiophene, C8BTBT, 30 nm, Sigma-Aldrich) in direct contact with the dielectric surface, (b) the emissive layer, where the electron–hole recombination and light generation occur, is a host–guest system (60 nm blend of CBP and DMAC-DPS, both materials from Ossila), and (c) the electron-transporting layer ( $\alpha,\omega$ -diperfluorohexyl-quarterthiophene, DFH-4T, 45 nm, Sigma-Aldrich). Drain (D) and source (S) electrodes (silver, 70 nm) are then deposited

**Table 1. Optoelectronic Properties of Organic Light-Emitting Multi-Layer Transistor Using CBP:DMAC-DPS Emissive Blends with Different DMAC-DPS Contents**

	unit	DMAC-DPS content (%)			
		5	10	15	20
hole current, $I_{DS@V_{DS,max}}$	$\mu\text{A}$	886	908	1150	981
electron current, $I_{DS@V_{DS,max}}$	$\mu\text{A}$	38	6.6	8.6	21.5
saturation hole mobility, <sup>a</sup> $\mu_{h,sat}$	$\text{cm}^2/(\text{V s})$	1.2	1.1	1.96	2.1
saturation electron mobility, <sup>a</sup> $\mu_{e,sat}$	$\text{cm}^2/(\text{V s})$	0.08	0.02	0.15	0.04
hole threshold, <sup>a</sup> $V_{th}^h$	V	-33.5	-25.4	-34.6	-26
electron threshold, <sup>a</sup> $V_{th}^e$	V	40.5	52.9	48.7	38.7
electroluminescence, EL@ $V_{DS,max}$	nW	4.7	7.5	32.5	6.3
external quantum efficiency, EQE@ $V_{DS,max}$	$10^{-3}$ %	0.25	0.42	1.38	0.3
ON/OFF	$\times 10^5$	3.05	1.16	1.31	1.36

<sup>a</sup>Forward sweep.

on top of the uppermost organic layer. Throughout this paper, we will refer to this device structure as 3L-OLET.

In such a multilayer heterostructure, the *p*- and the *n*-type semiconductors provide holes and electrons to the emissive layer under the effect of both external fields (Figure 2b). All values of HOMO and LUMO are considered from the literature. We refer the reader to refs 39 and 58 for more general considerations on these materials and their energetics in similar configurations.

Figure 2c shows the optoelectronic characterization (transfer characteristics) of organic light-emitting transistors using CBP:DMAC-DPS blends with the same thickness (60 nm) but different DMAC-DPS contents within the CBP host molecules (as labeled). We fabricated two substrates for each transistor configuration, with each substrate containing a total of 8 devices with a common gate. All devices have the same geometry (channel length and width), with organic semiconductor layers fabricated at the same time, with the only difference being the emissive layer and its guest content. The right *y*-axis in all panels reports the electroluminescence (EL) signal measured with a photodiode in direct contact with the substrate (bottom emission in our case). We show the same scale for both left and right *y*-axes in all panels for a more direct comparison. We recall that measured electroluminescence is only a part of the total light which is generated in the device. Measuring top emission (light extracted from the top of the device) is currently beyond our experimental capabilities. Within the same substrate, we observed a variability in performances between 5 and 10% among working devices.

All organic light-emitting transistors exhibit ambipolar behavior independently of the composition of the emissive layer (typical “V” shape of the *p*-transfer curve in all panels in Figure 2c). Hole transport is the dominating charge transport mechanism and it is approximately 2 orders of magnitude larger than the electron counterpart; within the range of applied bias (1100 V), this leads to an unbalanced charge transport in all devices. Ambipolar operation in our multilayer heterostructure transistor can be schematically represented as two vertically stacked organic thin-film transistors, each one carrying one type of charge (holes for the bottom C8BTBT layer and electrons for the topmost DFH-4T layer).

During the  $I_{DS}$ - $V_G$  sweep (at  $V_{DS} = -100$  V, Figure 2.d), electroluminescence is observed under two distinct regimes: (a) when charge transport is governed solely by holes within the device (right-hand side of the black curve) and (b) in proximity of the curve apex, where both transistors operate in their ON-state and more equilibrated distribution of charges is

achieved. In this latter regime, an increasing population of minority electrons originating from the *n*-type semiconductor layer is injected and transported laterally toward the recombination region. In ambipolar transistors, the drain-source current  $I_{DS}$  in the saturation region can be described as

$$I_{DS,sat} = \frac{W_{ch}}{2L_{ch}} [\mu_{e,sat} C_i (V_G - V_{th,e})^2 + \mu_{h,sat} C_i (V_{DS} - (V_G - V_{th,h}))^2] \quad (1)$$

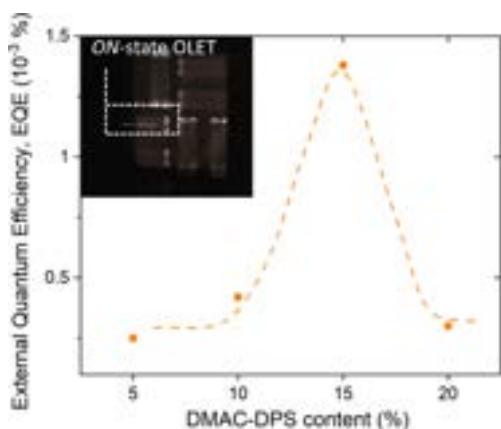
where  $C_i$  (6.6 nF/cm<sup>2</sup> for PMMA) is the capacitance per unit area of the dielectric layer,  $\mu_{sat}$  and  $V_{th}$  are the device saturation mobility and threshold voltages for holes (*h*) and electrons (*e*), and  $W_{ch}$  (5 mm) and  $L_{ch}$  (100  $\mu\text{m}$ ) are the transistor channel width and length, respectively.

Table 1 summarizes the optoelectronic properties of 3L-OLETs using CBP:DMAC-DPS blends with different DMAC-DPS contents. At the largest applied bias ( $V_{DS,max} = V_{G,max} = 1100$  V), we observed a variation of approximately <15% between hole and electron currents among different DMAC-DPS doping contents. Field-effect saturation mobility and threshold voltage are calculated from the linear fit of  $\sqrt{\frac{2L_{ch}}{W_{ch}C_i} I_{DS,sat}}$  (forward sweep of the  $I_{DS}$  vs  $V_G = V_{DS}$ ). We found values of hole (electron) mobilities of 1–2 (0.02–0.15)  $\text{cm}^2/(\text{V s})$  (see Table 1), which are approximately 1 order of magnitude smaller than those of the single-layer organic field-effect transistor counterpart. We refer the reader to one of our earlier works using the same set of materials.<sup>59</sup>

Threshold voltages found ( $[-36, -25]$  V for holes and  $[38, 53]$  V for electrons) are consistent with OLETs using a low-*k* dielectric layer such as PMMA.<sup>60</sup> Larger variation in the case of the holes among different guest concentrations might be due to the dielectric interface affecting both charge injection and transport within the stack. Within the range of our applied voltage, all transistors exhibit negligible gate leakage currents ( $\sim$ few tens of nA), which is several orders of magnitude lower than the largest drain-source current,  $I_{DS,max}$  and values of ON/OFF ratio of the order of  $10^5$ , calculated in the limit of unipolar regime (consistent with values previously reported for ambipolar devices). Both mobility and threshold values do not exhibit seemingly any clear dependence on the DMAC-DPS content within the emissive blend. We also observed a non-negligible hysteresis in all of the OLETs, with a constant shift of approximately 8–9 V toward higher bias (considering the apex as a reference point). Measured light output closely follows this behavior and it is consistent with previous

observations on multilayer heterostructures using similar sets of materials.<sup>61</sup> We anticipate this to be related to different injection regimes (holes vs. electrons) and possible charge trapping localized at the dielectric interfaces,<sup>62</sup> which might indirectly also affect the light generation mechanism; further, a more detailed investigation of this effect is currently ongoing.

Figure 3 shows the external quantum efficiency EQE (=emitted optical power/injected current) for our organic



**Figure 3.** External quantum efficiency (EQE) as a function of different DMAC-DPS contents within the emissive blend for multilayer organic light-emitting transistors. The dashed line is a guide-to-the-eye only. (Inset) Optical image of one of our representative OLET (emissive layer: CBP:DMAC-DPS 15%) in its ON-state.

light-emitting transistors as a function of DMAC-DPS content with the emissive layer, as calculated from transfer curves in Figure 2c. We recall that these values are overall an underestimate of the real efficiency of devices, since we are currently limited to the measurement of only bottom emission for our devices. Table T1 (Supporting Information) compares the present work with other works in the literature for light-emitting transistors using TADF emitters. We found that 3L OLETs with 15% DMAC-DPS content is the most efficient emissive blend, which is approximately 3–5 times larger than the other concentrations. We note that for this structure we also found the largest values of *field-effect* mobilities of the device for both holes and electrons.

The inset of Figure 3 shows the light generated in our device (bottom emission) in one of our representative devices in its ON-state. For all of our devices, we found that the efficiency remains approximately the same in the saturation regime, independent of the applied gate voltage (Figure S3, Supporting Information).

For a given organic semiconductor, molecular packing and intermolecular interactions critically determine both electronic transport and optical performance.<sup>63</sup> To directly compare optical and device properties, the blends used for spectroscopic studies (Figure 1) were prepared at the same time with those integrated into the 3L-OLET architecture (Figure 2c), with deposition carried out on different substrates: quartz for optical characterization and a C8BTBT layer on a PMMA dielectric for device fabrication. Figure 4 shows the surface structure of each organic layer within the multilayer trilayer organic stack investigated by atomic force microscopy (AFM). Each panel

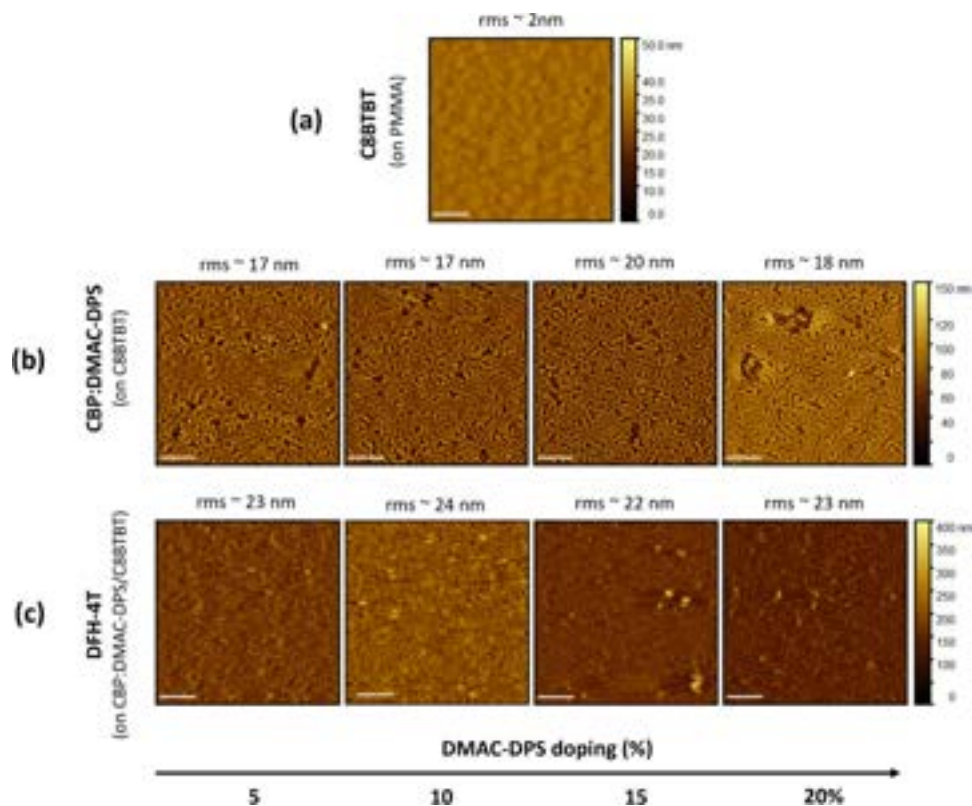


**Figure 4.** Atomic force microscopy (AFM) images of (a) C8BTBT deposited on PMMA, (b) emissive blends deposited on C8BTBT with different DMAC-DPS contents, and (c) DFH-4T deposited on each blend in (b). The image size ( $10\ \mu\text{m} \times 10\ \mu\text{m}$ ) and scale bar ( $2\ \mu\text{m}$ ) are the same for all micrographs. The arrow indicates increasing concentration of DMAC-DPS in the blend (as labeled). Roughness values (rms) are also reported.

also reports the average surface roughness of the layer (rms, root-mean square value). The image scan size is  $10\ \mu\text{m} \times 10\ \mu\text{m}$ , and the scale bar is  $2\ \mu\text{m}$  for all micrographs.

Figure 4a reveals the *island-like* structure of C8BTBT on PMMA, consistent with the growth mechanism reported in earlier studies.<sup>64</sup> The film displays an exceptionally smooth surface (rms <2 nm) with large, interconnected grains, indicative of efficient  $\pi$ - $\pi$  stacking and reduced grain boundary scattering. Such morphological features are highly advantageous for charge transport, providing percolation pathways, leading to the large hole mobility observed in the multilayer heterostructure.

Deposition of the emissive layer retrace the underlying C8BTBT surface (Figure 4b), as we have already observed in some of our previous works deposited on the same *p*-type layer.<sup>65</sup> All surfaces exhibit very similar structures and values of surface roughness (17–20 nm) with no clear dependence on the DMAC-DPS content within the host. In the case of a host triplet energy closer to the ones of the guest (or slightly higher), a uniform distribution of the guest within the host matrix at the molecular level can lead to the reduction of the average time and distance for host–guest triplet energy transfer, thus potentially improving the utilization of triplet excitons, while also reducing charge quenching (CQ) and triplet–triplet annihilation (TTA).<sup>66</sup> Based on similarity-intermiscibility theory and because of their similar shape/configuration, CBP and DMAC-DPS can lead to a uniform dispersion of DMAC-DPS in CBP during the thin film fabrication process. Fan et al., on the other hand, reported large roughness for a neat DMAC-DPS film due to the strong intermolecular interaction induced crystallization and aggregation.<sup>67</sup> When the electron-transporting layer (DFH-4T) is deposited on the topmost surface (Figure 4c), the underlying surface and structure of the emissive layer appear to be completely buried. We observed an overall increased surface roughness (rms  $\sim$  22–24 nm) and no correlation with the guest concentration. While a rough DFH-4T surface can lead to more efficient charge injection from the electrodes, our results suggest that a difference in contact resistance between the layer and the topmost electrode, if any, can be neglected. We also report the surface morphology of a single DFH-4T layer deposited directly on PMMA as reference (Figure S4, Supporting Information). In summary, the morphological analysis of different interfaces within the device shows no major differences within the active organic stack.

Intramolecular charge transfer (ICT) between the host (CBP) and the guest (DMAC-DPS) at the interface between the emissive layer and the electron-transport layer should be considered, which can give rise to the formation of a low-energy exciplex.<sup>68,69</sup> Based on morphological studies (Figure 4), electron injection should be favored at the interface DFH-4T/metal; in fact, a rougher surface (i.e., DFH-4T) can lead to a more efficient injection mechanism due to the actual contact area (consistent with the electrode fabrication process) and hotspots (nanoscale regions where field is locally enhanced).<sup>70</sup> Also, an unbalanced transport (holes are predominant in the device) will lead to light being generated closer to the drain electrode, where increased charge-exciton quenching can occur.<sup>71</sup>

While the overall surface morphology does not exhibit any macroscopic variation depending on DMAC-DPS content within the blends (Figure 4), differences in the shapes of both the host and guests and their dispersion in a blend can play a

role in the charge transport at the nanoscale. Recent works,<sup>72</sup> including one of ours,<sup>61</sup> have suggested that the improved electroluminescence for a specific host–guest blend can result from either a pure improved optical response or improved electrical properties of the blend itself. In this study, the former is highly unlikely; very low values of PLQY have been for example reported for CBP:DMAC-DPS blends, which further decrease with increasing guest concentration,<sup>73</sup> and emission following optical and electrical excitation shows a different trend as a function of the DMAC-DPS content (Figure S2, Supporting Information).

**Electronic (Field-Effect) Properties of CBP:DMAC-DPS Blends.** To study the electronic properties of the emissive blends, we have fabricated bottom-gate/top-contacts field-effect transistors, where the blend itself is the active layer. Figure 5 shows the  $I_{DS}$  vs.  $V_{DS}$  ( $=V_{GS}$ ) for both hole (left side)

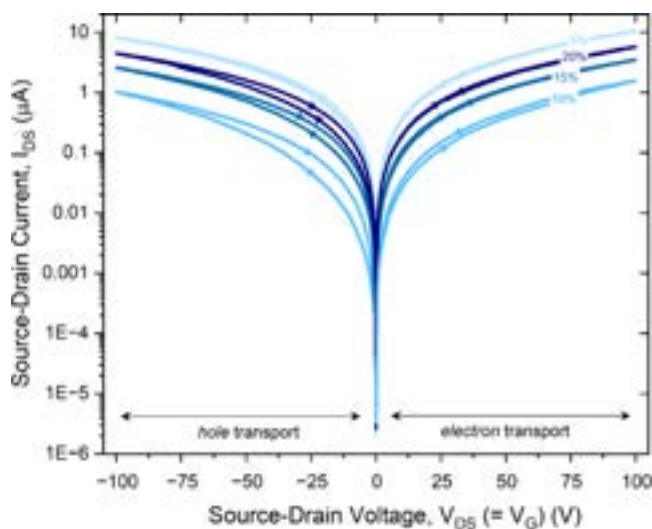


**Figure 5.**  $I_{DS}$  vs  $V_{DS}$  ( $=V_G$ ) curves of OFET with the blend as active layer showing the ambipolar nature of the blends for all DMAC-DPS contents. Sweep directions and DMAC-DPS contents are as labeled.

and electron (right side) curves of CBP-DMAC-DPS blends OFETs (60 nm thickness, same as in multilayer OLETs) for different DMAC-DPS contents; these transistors have the same geometry as the OLETs in Figure 2 ( $W_{ch}$  = 5 mm and  $L_{ch}$  =  $100\ \mu\text{m}$ , PMMA dielectric). Sweeps for both holes and electrons are shown and labeled accordingly, as well as the DMAC-DPS doping concentration within the blends. We observed that all blends show an overall very balanced transport for both holes and electrons. Time-of-flight (ToF) studies have shown that CBP exhibits a value of mobility of  $2 \times 10^{-3}$  ( $3 \times 10^{-4}$ )  $\text{cm}^2/(\text{V s})$  for holes (electrons)<sup>74</sup>. TADF emitters often exhibit both hole and electron transport properties as a result of their intrinsic molecular structure (acceptor–donor–acceptor). The HOMO level of the DMAC-DPS is close to that of *p*-type host CBP; thus, holes tend to be transported on the host molecule in these blends.

We found that these transistors, while exhibiting *field-effect* response in the range of our biases ( $\pm 100$  V), do not emit light, suggesting that the presence of semiconducting layer(s) is a key enabling component for light emission (exciton creation and decay);<sup>75</sup> also the hole charge transport shows a larger hysteresis compared to the electron counterpart, indicating some larger trapping mechanism at the dielectric interface. A more detailed analysis of the electronic properties of our

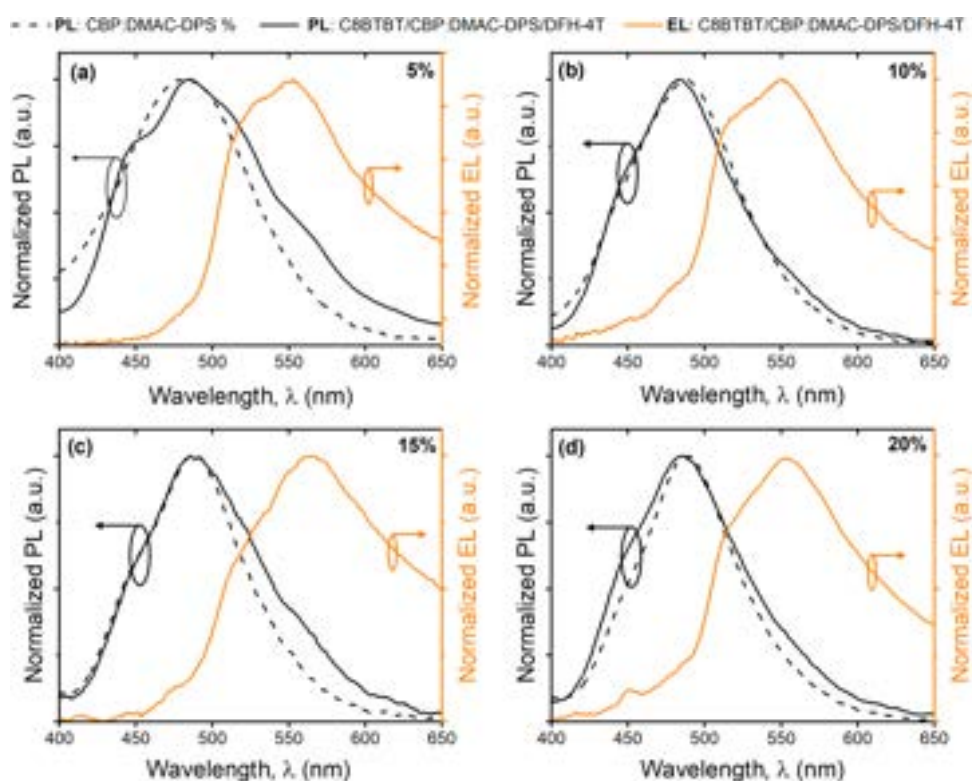


**Figure 6.** (Left y-axis) Normalized photoluminescence of CBP:DMAC-DPS blends on quartz (dashed lines) and in a multilayer stack (solid line) and (right y-axis) normalized electroluminescence spectra in 3L-OLET for (a) 5%, (b) 10%, (c) 15%, and (d) 20% DMAC-DPS content within the emissive blend showing a red shift of the main emission peak, depending on type of excitation.

blends shows a constantly larger electron conduction contribution than the hole properties; interestingly, we found also that the largest contribution of electron transport to the blend transport occurs for the emissive blend with 15% DMAC-DPS ( $I_e/I_h @|100| V = 1.51$ , see Table T2, Supporting Information). While these blends have been deposited at the same time as the device in Figure 2, these are potentially not the same blends since these are deposited directly on the PMMA surface (as compared to onto the C8BTBT layer), where morphology and interfaces are different (not shown). While these experimental results represent one of the few reported measurements of electronic properties in emissive blends, further investigation is certainly needed to further elucidate how the blend electronic properties can affect the overall light generated in the device in the limit of a field-effect transport regime (i.e., emissive layer thickness variation, more guest concentrations, measurement of mobility with Time-of-flight experiments). In fact, we believe that a greater electron contribution can potentially favor the exciton formation within the blends when in a multilayer heterostructure, thus leading to a larger electroluminescence in OLET devices as well as preventing charge-exciton quenching mechanisms, including the electro-oxidation effect.<sup>76</sup> These results clearly indicate the key role played by not only the optical properties but also the electronic properties of the blend for device electroluminescence.

**Optical and Electrical Excitation in CBP:DMAC-DPS Blends.** Figure 6 shows the electroluminescence of our 3L-OLET devices using different CBP:DMAC-DPS blends with (a) 5%, (b) 10%, (c) 15%, and (d) 20% DMAC-DPS contents (same devices as in Figure 2 and Figure 3). Photoluminescence spectra for the same multilayer stack (solid line) and for the

blends on quartz (dashed line, data from Figure 1) are also reported as reference. While we observed minor differences between the photoluminescence of the blends on quartz and within the multilayer heterostructure, we found a clear (red) shift between optical excitation (black curves) and electrical excitation (orange curves). Seemingly, we found no dependence of the value of this shift on the concentration; however, we note that the largest shift occurs in the case of the most efficient device (also the largest amount of light generated).

With its rigid, planar biphenyl core with two electron-rich carbazole units attached at the 4- and 4'-positions, CBP can undergo noncovalent dimerization or aggregation through  $\pi$ - $\pi$  interactions between carbazole units in the solid state or at high concentrations. This can introduce new low-energy excited states (typically excimers) that emit at wavelengths longer than those of the monomeric emission, thus resulting in red-shifted and broadened emission and altered energy transfer dynamics. In such a case, we would expect the spectral shift to be present in both photoluminescence and electroluminescence.

On the other hand, any type of excitation process can lead to the formation of excitons inside the organic material, with the nature of the excited states determining the emission spectra. In organic semiconductors, bimolecular excited states can form through the interaction of excited and ground-state donor-acceptor molecules, involving charge or energy exchange; in the case of the same (different) molecule, the resulting excited state is called the excimer (exciplex). Both are well reported in the literature<sup>77</sup> and can form under either optical or electrical excitation. However, electromers and electroplexes, two other types of charge-transfer complexes, are typically observed only under electrical excitation. Their formation tends to occur in

systems with planar, tightly packed molecules, where charge recombination between neighboring sites is more likely,<sup>78</sup> or in materials with a high net dipole moment, where an external electric field can polarize the molecular environment. This can shift energy levels, stabilize intermediate states, and create favorable conditions for forming these electrically induced species.<sup>79</sup> Such polarization effects do not occur under optical excitation, this being the reason these species are not seen in photoluminescence experiments.

In the case of the blends deposited on quartz (Figure 1), the photoluminescence spectrum is characteristic of exciplex emission arising from host–guest interaction. This suggests that the emissive state originates from the interaction between the donor and acceptor components within the blend. A similar PL emission profile is retained in the three-layer configuration, where both electron and hole semiconductor layers are introduced, indicating that the added layers do not significantly perturb the photophysics response of the system under optical excitation (Table T3, Supporting Information). While the emission intensity varies, the peak position does not shift appreciably, implying that the same emissive states are populated regardless of structural complexity under photoexcitation. On the other hand, electroluminescence spectra exhibit a significant red shift in the emission peak (~65–80 nm) for the different concentrations of DMAC-DPS in the blend, with the highest efficiency leading to the most red-shifted spectrum. This concentration-dependent spectral evolution strongly suggests the formation of new emissive states, distinct from the photoexcited exciplex. Further, the study of the dependence of the electroluminescence from the applied gate bias at a constant  $V_{DS} = -100$  V for such 3L-OLET (with CBP:DMC-DPS 15% blend, Figure S5 in the Supporting Information) shows a variation of its amplitude from the bias; however, all detectable EL spectra exhibit the red-shifted main emission component. In addition, the absence of light emission in the OFET blend configuration (Figure 5) as well as no observed shift when the *n*-type layer is removed from the device multilayer structure (not shown, currently under study) both suggest that this emission originates from an electroplex formed at the interface between the blend and the electron-transporting layer, where charges are indeed moving horizontally under the field-effect. While this is consistent with our observations in organic light-emitting transistors, further investigations are currently ongoing to elucidate in more detail the spectral change upon electrical excitation in our devices.

## CONCLUSION

In summary, we have investigated the optical and electronic behavior of multilayer organic heterostructures incorporating the TADF emitter DMAC-DPS in a CBP matrix, in the limit of *field-effect* conditions in transistor architectures. Our findings reveal two key outcomes: first, a 15% DMAC-DPS content yields the highest electroluminescence efficiency, attributed to improved and balanced charge transport within the emissive blend; second, electrical excitation leads to a significant red-shift in the emission spectrum, consistent with the formation of electroplexes at the interface between the emissive layer and the *electron-transport* semiconductor. These results highlight the importance of both blend composition and interfacial effects in optimizing electroluminescence in TADF-based organic light-emitting transistors.

## EXPERIMENTAL METHODS

**Device Fabrication and Characterization.** Glass/ITO substrates were carefully cleaned to ensure high-quality film deposition. The cleaning sequence involved sonication in diluted Hellmanex III (10 min), deionized water (5 min), acetone (two cycles of 10 min), and 2-propanol (10 min), followed by drying under nitrogen flow. To further improve surface wettability and remove residual organic contaminants, the substrates were treated with oxygen plasma (15 min, 100 W) prior to dielectric coating. PMMA (Allresist AR-P 669.06) dielectric layers were then deposited by spin-coating and annealed on a hot plate at 110 °C for 30 min in ambient air, a step that ensured solvent removal and stabilized the polymer layer. Film thicknesses of both dielectric and organic layers were determined using a stylus profilometer (Dektak/XT), while surface morphology was examined by atomic force microscopy (AFM, Bruker Dimension Icon) over a 10  $\mu\text{m} \times 10 \mu\text{m}$  scan area. Device fabrication was carried out in a Moorfield Nanotechnology MiniLab90, equipped with four low-temperature evaporation sources for organics and two thermal sources for metals, operating at a base pressure of  $\sim 10^{-7}$  mbar.

For optical studies, DMAC-DPS thin films (30 nm, deposition rate 0.15 Å/s) and CBP:DMAC-DPS emissive blends (60 nm) were deposited on precleaned quartz substrates under high vacuum ( $5 \times 10^{-7}$  mbar). The deposition rate of the CBP host was fixed at 1 Å/s for all blends, while the DMAC-DPS guest rate was adjusted to obtain the desired composition.

Electro-optical characterization was performed inside a nitrogen glovebox at room temperature by using a custom-built setup coupled to a Keysight B1500A semiconductor parameter analyzer. The emitted light was collected in a bottom-emission configuration with a calibrated Hamamatsu S1337 photodiode placed in direct contact with the substrate, thereby enabling accurate quantification of light output directly through the transparent electrode and substrate. Electroluminescence spectra were recorded by using a Konica Minolta CS-2000 spectroradiometer.

**Photoluminescence Studies.** Fluorescence spectra were obtained with a custom spectroscopy setup based on a continuous-wave He–Cd gas laser (Plasma HCCL-15UM). Pump radiation (325 nm, 15 mW) was spectrally filtered (short-pass 400 nm and bandpass 325 nm filters) to suppress the radiation from the nonlasing plasma discharge lines, attenuated, and focused on the sample surface using an aluminum *off-axis* parabolic mirror (25.4 mm reflective focal length). Power delivered to the sample was in the 1–10  $\mu\text{W}$  range. Photoluminescence was collected using a custom-built spectroscopic system, including a He–Cd laser ( $\lambda_{\text{exc}} = 325$  nm) as the excitation source and an IR2000 spectrometer to collect the emitted light. Spectra were recorded in the 400–800 nm range with 1 s exposure time. An optical density (OD) 2.0 filter was incorporated into the optical path to mitigate potential high excitation power effects.

## ASSOCIATED CONTENT

### Supporting Information

The Supporting Information is available free of charge at <https://pubs.acs.org/doi/10.1021/acsphotonics.5c01335>.

Mechanism of thermally-activated delayed fluorescence (TADF), photoluminescence vs DMAC-DPS content in

CBP:DMAC-DPS blends, external quantum efficiency dependence from bias in 3L-OLETs, surface morphology of n-type organic semiconductor layer, electrical characterization of CBP:DMAC-DPS blend-based OFET, and luminescence properties in CBP:DMAC-DPS blends under optical and electrical excitation (PDF)

## AUTHOR INFORMATION

### Corresponding Author

**Caterina Soldano** – Department of Electronics and Nanoengineering, School of Electrical Engineering, Aalto University, 02150 Espoo, Finland; Department of Physics, Northeastern University, Boston, Massachusetts 02115, United States; [orcid.org/0000-0001-6345-290X](https://orcid.org/0000-0001-6345-290X); Email: [caterina.soldano@aalto.fi](mailto:caterina.soldano@aalto.fi)

### Authors

**Ornella Laouadi** – Department of Electronics and Nanoengineering, School of Electrical Engineering, Aalto University, 02150 Espoo, Finland

**Vladimir Kornienko** – Department of Electronics and Nanoengineering, School of Electrical Engineering, Aalto University, 02150 Espoo, Finland; [orcid.org/0000-0002-5157-3218](https://orcid.org/0000-0002-5157-3218)

**Katherine Gallegos-Rosas** – Department of Electronics and Nanoengineering, School of Electrical Engineering, Aalto University, 02150 Espoo, Finland; [orcid.org/0000-0001-8561-5722](https://orcid.org/0000-0001-8561-5722)

**Amirhossein Azari** – Department of Electronics and Nanoengineering, School of Electrical Engineering, Aalto University, 02150 Espoo, Finland

Complete contact information is available at:

<https://pubs.acs.org/10.1021/acsp Photonics.Sc01335>

### Author Contributions

C.S. conceived and carried out most of the experiments, analyzed the data and wrote the manuscript. K.G.-R. and A.A. supported through additional experiments, AFM studies, data analysis and validation. V.K. and O.L. contributed to the optical characterization. C.S. supervised the project. All authors contributed to the manuscript, provided feedback, and have given approval to its final version.

### Funding

The authors acknowledge financial support from the Research Council of Finland: Flagship Program PREIN-grant #320167, TADF-Field-grant #355992, WALLPAPER-grant #352914 and CarbonSurf-grant #329406.

### Notes

The authors declare no competing financial interest.

## ACKNOWLEDGMENTS

The authors would like to thank the support received from Micronova Nanofabrication Centre (Espoo, Finland) and OtaNano research infrastructure at Aalto University.

## REFERENCES

- (1) Horowitz, G. Organic Field Effect Transistors. *Adv. Mater.* **1998**, *10*, 365–377.
- (2) Burroughes, D. M.; Bradley, D. D. C.; Brown, A. R.; Marks, R. N.; Mackay, K.; Friend, R. H.; Burns, P. L.; Holmes, A. B. Light-emitting diodes based on conjugated polymers. *Nature* **1990**, *347*, 539–541.
- (3) Zhang, C.; Chen, P.; Hu, W. Organic Light-Emitting Transistors: Materials, Device Configurations, and Operations. *Small* **2016**, *12*, 1252–1294.
- (4) Baldo, M. A.; Lamansky, S.; Burrows, P. E.; Thompson, M. E.; Forrest, S. R. Very high-efficiency green organic light-emitting devices based on electrophosphorescence. *Appl. Phys. Lett.* **1999**, *75* (1), 4–6.
- (5) Schmidbauer, S.; Hohenleutner, A.; König, B. Chemical Degradation in Organic Light-Emitting Devices: Mechanisms and Implications for the Design of New Materials. *Adv. Mater.* **2013**, *25*, 2114–2129.
- (6) Volz, D.; Wallech, M.; Fléchon, C.; Danz, M.; Verma, A.; Navarro, J. M.; Zink, D. M.; Bräse, S.; Baumann, T. From iridium and platinum to copper and carbon: new avenues for more sustainability in organic light-emitting diodes. *Green Chem.* **2015**, *17*, 1988–2011.
- (7) Xu, Y.; Xu, P.; Hu, D.; Ma, Y. Recent progress in hot exciton materials for organic light-emitting diodes. *Chem. Soc. Rev.* **2021**, *50*, 1030–1069.
- (8) Shi, Y.-Z.; Wu, H.; Wang, K.; Yu, J.; Ou, X.-M.; Zhang, X.-H. Recent progress in thermally activated delayed fluorescence emitters for nondoped organic light-emitting diodes. *Chem. Sci.* **2022**, *13*, 3625–3651.
- (9) Nakanotani, H.; Higuchi, T.; Furukawa, T.; Masui, K.; Morimoto, K.; Numata, M.; Tanaka, H.; Sagara, Y.; Yasuda, T.; Adachi, C. High-efficiency organic light-emitting diodes with fluorescent emitters. *Nat. Commun.* **2014**, *5*, 4016.
- (10) Noda, H.; Nakanotani, H.; Adachi, C. Excited state engineering for efficient reverse intersystem crossing. *Sci. Adv.* **2018**, *4* (6), No. ea06910.
- (11) Karthik, D.; Jung, Y. H.; Lee, H.; Hwang, S.; Seo, B. M.; Kim, J. Y.; Han, C. W.; Kwon, J. H. Acceptor–Donor–Acceptor-Type Orange–Red Thermally Activated Delayed Fluorescence Materials Realizing External Quantum Efficiency Over 30% with Low Efficiency Roll-Off. *Adv. Mater.* **2021**, *33*, 2007724.
- (12) Zhang, C.; Zhang, D. D.; Bin, Z. Y.; Liu, Z. Y.; Zhang, Y. W.; Lee, H.; Kwon, J. H.; Duan, L. Color-Tunable All-Fluorescent White Organic Light-Emitting Diodes with a High External Quantum Efficiency Over 30% and Extended Device Lifetime. *Adv. Mater.* **2022**, *34*, 2103102.
- (13) Park, I. S.; Min, H.; Kim, J. U.; Yasuda, T. Deep-Blue OLEDs Based on Organoboron-Phenazasiline-Hybrid Delayed Fluorescence Emitters Concurrently Achieving 30% External Quantum Efficiency and Small Efficiency Roll-Off. *Adv. Optical Mater.* **2021**, *9*, 2101282.
- (14) Uoyama, H.; Goushi, K.; Shizu, K.; Nomura, H.; Adachi, C. Highly efficient organic light-emitting diodes from delayed fluorescence. *Nature* **2012**, *492*, 234–238.
- (15) He, Z.; Wang, C.; Zhao, J.; Du, X.; Yang, H.; Zhong, P.; Zheng, C.; Lin, H.; Tao, S.; Zhang, X. Blue and white solution-processed TADF-OLEDs with over 20% EQE, low driving voltages and moderate efficiency decrease based on interfacial exciplex hosts. *J. Mater. Chem. C* **2019**, *7*, 11806–11812.
- (16) Zhao, G.; Liu, D.; Wang, P.; Huang, X.; Chen, H.; Zhang, Y.; Zhang, D.; Jiang, W.; Sun, Y.; Duan, L. Exceeding 30% External Quantum Efficiency in Non-doped OLEDs Utilizing Solution Processable TADF Emitters with High Horizontal Dipole Orientation via Anchoring Strategy. *Angew. Chem., Int. Ed.* **2022**, *61* (45), No. e202212861.
- (17) Godumala, M.; Choi, S.; Cho, M. J.; Choi, D. H. Recent breakthroughs in thermally activated delayed fluorescence organic light emitting diodes containing non-doped emitting layers. *J. Mater. Chem. C* **2019**, *7*, 2172–2198.
- (18) Zhang, D.; Song, X.; Cai, M.; Kaji, H.; Duan, L. Versatile Indolocarbazole-Isomer Derivatives as Highly Emissive Emitters and Ideal Hosts for Thermally Activated Delayed Fluorescent OLEDs with Alleviated Efficiency Roll-Off. *Adv. Mater.* **2018**, *30*, 1705406.
- (19) Wang, K.; Zheng, C.-J.; Liu, W.; Liang, K.; Shi, Y.-Z.; Tao, S.-L.; Lee, C.-S.; Ou, X.-M.; Zhang, X.-H. Avoiding Energy Loss on TADF Emitters: Controlling the Dual Conformations of D–A

Structure Molecules Based on the Pseudoplanar Segments. *Adv. Mater.* **2017**, *29*, 1701476.

(20) Chen, Y.; Zhang, D.; Zhang, Y.; Zeng, X.; Huang, T.; Liu, Z.; Li, G.; Duan, L. Approaching Nearly 40% External Quantum Efficiency in Organic Light Emitting Diodes Utilizing a Green Thermally Activated Delayed Fluorescence Emitter with an Extended Linear Donor-Acceptor-Donor Structure. *Adv. Mater.* **2021**, *33* (44), No. e2103293.

(21) Jiang, P.; Miao, J.; Cao, X.; Xia, H.; Pan, K.; Hua, T.; Lv, X.; Huang, Z.; Zou, Y.; Yang, C. Quenching-Resistant Multiresonance TADF Emitter Realizes 40% External Quantum Efficiency in Narrowband Electroluminescence at High Doping Level. *Adv. Mater.* **2022**, *34* (3), 2106954.

(22) Kim, H. M.; Choi, J. M.; Lee, J. Y. Blue thermally activated delayed fluorescent emitters having a bicarbazole donor moiety. *RSC Adv.* **2016**, *6*, 64133–64139.

(23) Cui, L.-S.; Ruan, S.-B.; Bencheikh, F.; Nagata, R.; Zhang, L.; Inada, K.; Nakanotani, H.; Liao, L.-S.; Adachi, C. Long-lived efficient delayed fluorescence organic light-emitting diodes using n-type hosts. *Nat. Commun.* **2017**, *8*, 2250.

(24) Nakanotani, H.; Masui, K.; Nishide, J.; Shibata, T.; Adachi, C. Promising operational stability of high-efficiency organic light-emitting diodes based on thermally activated delayed fluorescence. *Sci. Rep.* **2013**, *3*, 2127.

(25) Tsang, D. K.; Matsushima, T.; Adachi, C. Operational stability enhancement in organic light-emitting diodes with ultrathin Liq interlayers. *Sci. Rep.* **2016**, *6*, 22463.

(26) Ullah, M.; Armin, A.; Tandy, K.; Yamben, S. D.; Brun, P. L.; Meredith, P.; Namdas, E. B. Defining the light emitting area for displays in the unipolar regime of highly efficient light emitting transistors. *Sci. Rep.* **2015**, *5*, 8818.

(27) Sobus, J.; Bencheikh, F.; Mamada, M.; Wawrzinek, R.; Ribierre, J.-C.; Adachi, C.; Lo, S.-C.; Namdas, E. B. High Performance p- and n-Type Light-Emitting Field-Effect Transistors Employing Thermally Activated Delayed Fluorescence. *Adv. Funct. Mater.* **2018**, *28*, 1800340.

(28) Chaudhry, M. U.; Muhieddine, K.; Wawrzinek, R.; Sobus, J.; Tandy, K.; Lo, S. C.; Namdas, E. B. Organic Light-Emitting Transistors: Advances and Perspectives. *Adv. Fct. Mater.* **2020**, *30* (20), 1905282.

(29) Zaumseil, J.; Friend, R. H.; Sirringhaus, H. Spatial control of the recombination zone in an ambipolar light-emitting organic transistor. *Nat. Mater.* **2006**, *5*, 69–74.

(30) Liu, B.; McCarthy, M. A.; Iheanacho, B.; Wong, W. S.; Rinzler, A. G. Recent Developments of Carbon Nanotube Enabled Vertical Organic Light Emitting Transistors for OLED Displays. *SID Symp. Dig. of Technol. Papers* **2013**, *44* (1), 251–253.

(31) Hsieh, H. H.; Chen, W.-C.; Generali, G.; Soldano, C.; D'Alpaos, R.; Turatti, G.; Biondo, V.; Muccini, M.; Huitema, E.; Facchetti, A. Flexible Active-Matrix OLET Display on a Plastic Substrate, *SID Symp. Dig. of Technol. Papers* **2016**, *47* (1), 739–742.

(32) Prosa, M.; Benvenuti, E.; Kallweit, D.; Pellacani, P.; Toerker, M.; Bolognesi, M.; Lopez-Sanchez, L.; Ragona, V.; Marabelli, F.; Toffanin, S. Organic Light-Emitting Transistors in a Smart-Integrated System for Plasmonic-Based Sensing. *Adv. Funct. Mater.* **2021**, *31* (50), 2104927.

(33) Bronstein, H.; Nielsen, C. B.; Schroeder, B. C.; McCulloch, I. The role of chemical design in the performance of organic semiconductors. *Nat. Rev. Chem.* **2020**, *4*, 66–77.

(34) Quinn, J. T. E.; Zhu, J.; Li, X.; Wang, J.; Li, Y. Recent progress in the development of n-type organic semiconductors for organic field effect transistors. *J. of Mater. Chem. C* **2017**, *5*, 8654.

(35) Varghese, M. A.; Anshika, A.; Deivendran, H.; Nagarajan, N. Organic Light-Emitting Transistors: From Understanding to Molecular Design and Architecture. *ACS Appl. Electron. Mater.* **2021**, *3* (2), 550–573.

(36) Liu, Y.; Li, C.; Ren, Z.; Yan, S.; Bryce, M. R. All-organic thermally activated delayed fluorescence materials for organic light-emitting diodes. *Nat. Rev. Mater.* **2018**, *3*, 18020.

(37) Soldano, C. Engineering Dielectric Materials for High-Performance Organic Light Emitting Transistors (OLETs). *Materials* **2021**, *14* (13), 3756.

(38) Fahlman, M.; Fabiano, S.; Gueskine, V.; Simon, D.; Berggren, M.; Crispin, X. Interfaces in organic electronics. *Nat. Rev. Mater.* **2019**, *4*, 627–650.

(39) Capelli, R.; Toffanin, S.; Generali, G.; Usta, H.; Facchetti, A.; Muccini, M. Organic light-emitting transistors with an efficiency that outperforms the equivalent light-emitting diodes. *Nat. Mater.* **2010**, *9*, 496–503.

(40) Trukhanov, V. A.; Sosorev, A. Y.; Dominskiy, D. I.; Fedorenko, R. S.; Tafeenko, V. A.; Borshchev, O. V.; Ponomarenko, S. A.; Parashuk, D. Y. Dual Optoelectronic Organic Field-Effect Device: Combination of Electroluminescence and Photosensitivity. *Molecules* **2024**, *29* (11), 2533.

(41) Wu, Z.; Liu, Y.; Guo, E.; Darbndy, G.; Wang, S.-J.; Hubner, R.; Kloes, A.; Kleemans, H.; Leo, K. Efficient and low-voltage vertical organic permeable base light-emitting transistors. *Nat. Mater.* **2021**, *20*, 1007–1014.

(42) He, P.; Lan, L.; Deng, C.; Wang, J.; Peng, J.; Cao, Y. Highly efficient and stable hybrid quantum-dot light-emitting field-effect transistors. *Mater. Horiz.* **2020**, *7*, 2439–2449.

(43) Cho, S.-Y.; Kim, S.-Y.; Jeon, S.; Choi, R.; Lee, J.-H. A strategy to boost external quantum efficiency of organic light-emitting transistors. *Appl. Phys. Lett.* **2019**, *115*, 043301.

(44) Song, L.; Hu, Y.; Liu, O. Z.; Lv, Y.; Guo, X.; Liu, X. Harvesting Triplet Excitons with Exciplex Thermally Activated Delayed Fluorescence Emitters toward High Performance Heterostructured Organic Light-Emitting Field Effect Transistors. *ACS Appl. Mater. Interfaces* **2017**, *9*, 2711–2719.

(45) Sobus, J.; Bencheikh, F.; Mamada, M.; Wawrzinek, R.; Ribierre, J.-C.; Adachi, C.; Lo, S.-C.; Namdas, E. B. High Performance p- and n-Type Light-Emitting Field-Effect Transistors Employing Thermally Activated Delayed Fluorescence. *Adv. Funct. Mater.* **2018**, *28*, 1800340.

(46) Miao, Z.; Gao, C.; Shen, M.; Wang, P.; Gao, H.; Wei, J.; Deng, J.; Liu, D.; Qin, Z.; Wang, P.; Lei, Y.; Lo, S. C.; Zhang, X.; Yuan, G.; Namdas, E. B.; Ma, Y.; Dong, H.; Hu, W. Organic light-emitting transistors with high efficiency and narrow emission originating from intrinsic multiple-order microcavities. *Nat. Mater.* **2025**, *24*, 917.

(47) Ahmad, V.; Sobus, J.; Bencheikh, F.; Mamada, M.; Adachi, C.; Lo, S. C.; Namdas, E. B. High EQE and High Brightness Solution-Processed TADF Light-Emitting Transistors and OLEDs. *Adv. Opt. Mater.* **2020**, *8* (18), 2000554.

(48) Zhang, Q.; Li, B.; Huang, S.; Nomura, H.; Tanaka, H.; Adachi, C. Efficient blue organic light-emitting diodes employing thermally activated delayed fluorescence. *Nat. Phot.* **2014**, *8*, 326–332.

(49) Han, M.; Chen, Y.; Xie, Y.; Zhang, F.; Li, X.; Huang, A.; Fan, Y.; Fan, Y.; Gong, Y.; Peng, Q.; Li, Q.; Ma, D.; Li, Z. 1.42-Fold Enhancement of Blue OLED Device Performance by Simply Changing Alkyl Groups on the Acridine Ring. *Cell Reports Physical Science* **2020**, *1* (11), 100252.

(50) Kim, G. W.; Bae, H. W.; Lampande, R.; Ko, I. J.; Park, J. H.; Lee, C. Y.; Kwon, J. H. Highly efficient single-stack hybrid cool white OLED utilizing blue thermally activated delayed fluorescent and yellow phosphorescent emitters. *Sci. Rep.* **2018**, *8*, 16263.

(51) Li, B.; Yang, Z.; Gong, W.; Chen, X.; Bruce, D. W.; Wang, S.; Ma, H.; Liu, Y.; Zhu, W.; Chi, Z.; Wang, Y. Intramolecular Through-Space Charge Transfer Based TADF-Active Multifunctional Emitters for High Efficiency Solution-Processed OLED. *Adv. Optical Mater.* **2021**, *9*, 2100180.

(52) Yadav, R. A. K.; Dubey, D. K.; Chen, S.-Z.; Liang, T.-W.; Jou, J.-H. Role of Molecular Orbital Energy Levels in OLED Performance. *Sci. Rep.* **2020**, *10*, 9915.

(53) Jang, E.-B.; Choi, G.-S.; Bae, E.-J.; Ju, B.-K.; Park, Y.-W. Doping-Free Phosphorescent and Thermally Activated Delayed Fluorescent Organic Light-Emitting Diodes with an Ultra-Thin Emission Layer. *Nanomater.* **2023**, *13*, 2366.

- (54) Gong, S.; He, X.; Chen, Y.; Zuoquan, J.; Zhong, C.; Ma, D.; Qin, J.; Yang, C. Simple CBP isomers with high triplet energies for highly efficient blue electrophosphorescence. *J. Mater. Chem.* **2012**, *22*, 2894–2899.
- (55) Zhang, Q.; Tsang, D.; Kuwabara, H.; Hatae, Y.; Li, B.; Takahashi, T.; Lee, S. Y.; Yasuda, T.; Adachi, C. Nearly 100% Internal Quantum Efficiency in Undoped Electroluminescent Devices Employing Pure Organic Emitters. *Adv. Mater.* **2015**, *27*, 2096–2100.
- (56) Penfold, T. J.; Dias, F. B.; Monkman, A. P. The theory of thermally activated delayed fluorescence for organic light emitting diodes. *Chem. Commun.* **2018**, *54*, 3926–3935.
- (57) Gallegos-Rosas, K.; Azari, A.; Soldano, C. Carboxymethyl Cellulose as a Sustainable Dielectric Material for Organic Field-Effect Transistors. *ACS Appl. Elec. Mater.* **2025**, *7* (3), 1274.
- (58) Soldano, C.; Stefani, A.; Biondo, V.; Basirico, L.; Turatti, G.; Generali, G.; Ortolani, L.; Morandi, V.; Veronese, G. P.; Rizzoli, R.; Capelli, R.; Muccini, M. ITO-Free Organic Light-Emitting Transistors with Graphene Gate Electrode. *ACS Phot.* **2014**, *1* (10), 1082–1088.
- (59) Albeltagi, A.; Gallegos-Rosas, K.; Soldano, C. High-k Fluoropolymers Dielectrics for Low-Bias Ambipolar Organic Light Emitting Transistors (OLETs). *Materials* **2021**, *14*, 7635.
- (60) Soldano, C.; Generali, G.; Cianci, E.; Tallarida, G.; Fanciulli, M.; Muccini, M. Engineering organic/inorganic alumina-based films as dielectrics for red organic light-emitting transistors. *Thin Solid Films* **2016**, *616*, 408–414.
- (61) Soldano, C.; Laouadi, O.; Gallegos-Rosas, K. TCTA:Ir(ppy)<sub>3</sub> Green Emissive Blends in Organic Light-Emitting Transistors (OLETs). *ACS Omega* **2022**, *7* (48), 43719–43728.
- (62) Liu, C.; Xu, Y.; Li, Y.; Scheideler, W.; Minari, T. Critical Impact of Gate Dielectric Interfaces on the Contact Resistance of High-Performance Organic Field-Effect Transistors. *J. Phys. Chem. C* **2013**, *117*, 12337–12345.
- (63) Kitamura, M.; Arakawa, Y. Pentacene-based organic field-effect transistors. *J. Phys.: Condens. Matter* **2008**, *20*, 184011.
- (64) Moh, A. M.; Khoo, P. L.; Sasaki, K.; Watase, S.; Shinagawa, T.; Izaki, M. Growth and Characteristics of C8-BTBT Layer on C-Sapphire Substrate by Thermal Evaporation. *Phys. Status Solidi A* **2018**, *215*, 1700862.
- (65) Soldano, C.; D'Alpaos, R.; Generali, G. Highly Efficient Red Organic Light-Emitting Transistors (OLETs) on High-k Dielectric. *ACS Phot.* **2017**, *4* (4), 800–805.
- (66) Raišys, S.; Adomėnienė, O.; Adomėnas, P.; Rudnick, A.; Köhler, A.; Kazlauskas, K. Triplet Exciton Diffusion and Quenching in Matrix-Free Solid Photon Upconversion Films. *J. of Phys. Chem. C* **2021**, *125*, 3764–3775.
- (67) Fan, C.; Duan, C.; Wei, Y.; Ding, D.; Xu, H.; Huang, W. Dibenzothiophene-Based Phosphine Oxide Host and Electron-Transporting Materials for Efficient Blue Thermally Activated Delayed Fluorescence Diodes through Compatibility Optimization. *Chem. Mater.* **2015**, *27* (14), 5131–5140.
- (68) Hung, W. Y.; Fang, G. C.; Chang, Y. C.; Kuo, T. Y.; Chou, P. T.; Lin, S. W.; Wong, K. T. Highly efficient bilayer interface exciplex for yellow organic light-emitting diode. *ACS Appl. Mater. Interfaces* **2013**, *5* (15), 6826–6831.
- (69) Wu, T.-L.; Liao, S.-Y.; Huang, P.-Y.; Hong, Z.-S.; Huang, M.-P.; Lin, C.-C.; Cheng, M.-J.; Cheng, C.-H. Exciplex Organic Light-Emitting Diodes with Nearly 20% External Quantum Efficiency: Effect of Intermolecular Steric Hindrance between the Donor and Acceptor Pair. *ACS Appl. Mater. Interfaces* **2019**, *11* (21), 19294–19300.
- (70) Lu, Z.-H.; Hu, J.-X.; Zhong, Y.-N.; Zhou, X.; Xu, C.; Gao, X.; Xu, J.-L.; Duhm, S.; Wang, S.-D. Carrier injection in organic electronics: Injection hotspot effect beyond barrier reduction effect. *Appl. Phys. Lett.* **2018**, *113*, 043302.
- (71) Prosa, M.; Benvenuti, E.; Pasini, M.; Giovanella, U.; Bolognesi, M.; Meazza, L.; Galeotti, F.; Muccini, M.; Toffanin, S. Organic Light-Emitting Transistors with Simultaneous Enhancement of Optical Power and External Quantum Efficiency via Conjugated Polar Polymer Interlayers. *ACS Appl. Mater. Interfaces* **2018**, *10* (30), 25580–25588.
- (72) Gao, M.; Lee, T.; Burn, P. L.; Mark, A. E.; Pivrikas, A.; Shaw, P. E. Revealing the Interplay between Charge Transport, Luminescence Efficiency, and Morphology in Organic Light-Emitting Diode Blends. *Adv. Funct. Mater.* **2020**, *30*, 1907942.
- (73) Wang, Z.; Zhao, J.; Zhou, C.; Qi, Y.; Yu, J. Enhancement of Förster energy transfer from thermally activated delayed fluorophores layer to ultrathin phosphor layer for high color stability in non-doped hybrid white organic light-emitting devices. *Chin. Phys. B* **2017**, *26*, 047302.
- (74) Kang, J.-W.; Lee, S.-Y.; Park, H.-D.; Jeong, W.-I.; Yoo, K. M.; Park, Y.-S.; Kim, J.-J. Low roll-off of efficiency at high current density in phosphorescent organic light emitting diodes. *Appl. Phys. Lett.* **2007**, *90* (22), 223508.
- (75) Zambianchi, M.; Benvenuti, E.; Bettini, C.; Zanardi, C.; Seeber, R.; Gentili, D.; Cavallini, M.; Muccini, M.; Biondo, V.; Soldano, C.; Generali, G.; Toffanin, S.; Melucci, M. Anthracene-based molecular emitters for non-doped deep-blue organic light emitting transistors. *J. Mater. Chem. C* **2016**, *4*, 9411–9417.
- (76) Cui, L.-S.; Deng, Y.-L.; Tsang, D. P.-K.; Jiang, Z.-Q.; Zhang, Q.; Liao, L.-S.; Adachi, C. Controlling Synergistic Oxidation Processes for Efficient and Stable Blue Thermally Activated Delayed Fluorescence Devices. *Adv. Mater.* **2016**, *28*, 7620–7625.
- (77) (a) Jenekhe, S. A.; Osaheni, J. A. Excimers and exciplexes of conjugated polymers. *Science* **1994**, *265*, 765. (b) Wang, J.; Zhang, X. Organic light-emitting diodes based on electromer-mediated heterojunctions. *Appl. Phys. Lett.* **2018**, *113*, 143301. (c) Zhu, J.; Li, W.; Han, L.; Chu, B.; Zhang, G.; Yang, D.; Chen, Y.; Su, Z.; Wang, J.; Wu, S.; Tsuboi, T. Very broad white-emission spectrum based organic light-emitting diodes by four exciplex emission bands. *Opt. Lett.* **2009**, *34*, 2946. (d) Sarma, M.; Wong, K.-T. Exciplex: An Intermolecular Charge-Transfer Approach for TADF. *ACS Appl. Mater. Int.* **2018**, *10*, 19279.
- (78) Kalinowski, J.; Giro, G.; Cocchi, M.; Fattori, V.; Di Marco, P. Unusual disparity in electroluminescence and photoluminescence spectra of vacuum-evaporated films of 1,1-bis((di-4-tolylamino)phenyl) cyclohexane. *Appl. Phys. Lett.* **2000**, *76*, 2352.
- (79) Uoyama, H.; Goushi, K.; Shizu, K.; Nomura, H.; Adachi, C. Highly efficient organic light-emitting diodes from delayed fluorescence. *Nature* **2012**, *492* (7428), 234.